Version of the attached file: Non-peer reviewed preprint submitted to EarthArxiv
Peer-reviewed status of the attached file: Non-peer reviewed
Citation for the pre-print file: Hiatt, M., W. Sonke, E.A. Addink, W.M. van Dijk, M. van Kreveld, T. Ophelders, K. Verbeek, J. Vlamin, B. Speckmann, M.G. Kleinhans (2019), Geometry and topology of estuary and braided river channel networks automatically extracted from topographic data, EarthArxiv.
Additional information: : This manuscript is a preprint and has been submitted to *Journal of Geophysical Research: Earth Surface* for publication. The manuscript version posted on EarthArxiv is non-peer reviewed and subsequent version of the manuscript may differ slightly from this version. If the manuscript is accepted for publication, the final typeset version will be available via the "Peer-reviewed Publication DOI" link on the right hand side of the web page. Please feel free to contact any of the authors, we welcome feedback.

Geometry and topology of estuary and braided river channel networks automatically extracted from topographic data

Matthew Hiatt[1,2], Willem Sonke[3], Elisabeth A. Addink[1], Wout M. van Dijk[1], Marc van Kreveld[4], Tim Ophelders[5], Kevin Verbeek[3], Joyce Vlaming[1], Bettina Speckmann[3], and Maarten G. Kleinhans[1]

[1]Department of Physical Geography, Faculty of Geosciences, Utrecht University, Utrecht, the Netherlands
[2]Department of Oceanography and Coastal Sciences, College of the Coast and Environment, Louisiana State University, Baton Rouge, USA
[3]Department of Mathematics and Computer Science, TU Eindhoven, Eindhoven, the Netherlands
[4]Department of Information and Computing Science, Utrecht University, Utrecht, the Netherlands
[5]Department of Computational Mathematics, Science and Engineering, Michigan State University, East Lansing, USA

Key Points:

- A new volume-based method enables extraction of multi-thread channel networks from bathymetry across bed level jumps
- Both network topology and geomorphic information can be extracted at a range of spatial scales
- Estuaries typically form a single dominant channel at the largest spatial scale, while braided rivers show no scaling break

Corresponding author: Matthew Hiatt, mhiatt1@lsu.edu

Abstract

Automatic and objective extraction of channel networks from topography in systems with multiple interconnected channels, like braided rivers and estuaries, remains a major challenge in hydrology and geomorphology. Representing channelized systems as networks provides a mathematical framework for analyzing transport and geomorphology. In this paper, we introduce a mathematically rigorous methodology and software for extracting channel network topology and geometry from digital elevation models (DEMs) and analyze such channel networks in estuaries and braided rivers. Channels are represented as network links, while channel confluences and bifurcations are represented as network nodes. We analyze and compare DEMs from the field and those generated by numerical modeling. We introduce a metric called the sand function that characterizes the volume of deposited material separating channels to quantify the spatial scale attributed to each link. Scale asymmetry is observed in the majority of links downstream of bifurcations, indicating geometric asymmetry and bifurcation stability. The length of links relative to system size scales with sand function scale to the power of 0.24-0.35, while the number of nodes decreases against system scale and does not exhibit power-law behavior. Link depth distributions indicate that the estuaries studied tend to organize around a deep main channel that exists at the largest scale while braided rivers have channel depths that are more evenly distributed across scales. The methods and results presented establish a benchmark for quantifying the topology and geometry of multi-channel networks from DEMs with an automatic and objective tool.

Plain Language Summary

Channels are features of the Earth's surface that carry water, sediment, nutrients, and organisms across the continents towards the coasts. Scientists have long recognized that knowing the shapes, sizes and connections of channels in rivers, estuaries and deltas is vital for predicting future change. A useful way to represent channels is with a network. However, automatically identifying channel networks from surface elevation has been a major challenge because channels display a wide range of different shapes, sizes, and patterns, and often have many intersections with other channels. We have developed a method for identifying channel networks from height maps. We first find the "lowest path" in a channel network, meaning the channel that is at generally lower elevations than all other channels. We subsequently find the next lowest paths, where the measure for channel separation is the volume of sand that needs to be displaced to join neighboring channels. This method allows us to identify the channel network. We show previously unknown similarities and differences between the channel networks of estuaries and wide rivers with sand bars. Our work helps researchers more fully understand and predict how channel networks develop and evolve.

1 Introduction

Channels are ubiquitous features of Earth's surface that are important pathways for the transport of water, solids, and solutes across landscapes, provide a range of ecosystem services, and support economic activity. Channel patterns range significantly in complexity, from single-thread, meandering rivers cutting across continents and the sea floor, to multi-thread channel systems that bifurcate and converge in braided rivers, estuaries, and deltas. These patterns exist over a range of spatial scales. Understanding and quantifying channel network patterns and geometry are vital precursors to predicting many important environmental processes including geomorphological change, water and sediment transport, and ecosystem dynamics. However, automated recognition of channels and their connections from bathymetry is not straightforward because most channel systems have large spatial and temporal variations in bed elevation, arrangement, and water depth.

Quantifying patterns, structure, and geometries of channels is necessary to understand and predict landscape dynamics. Networks, which are mathematical representations of objects and the connections among those objects [*Newman*, 2003, 2010], are useful representations of topology and geometry in channelized systems [e.g., *Benda et al.*, 2004; *Czuba and Foufoula-Georgiou*, 2014; *Dai and Labadie*, 2001; *Marra et al.*, 2014; *Maidment*, 2016; *Rodriguez-Iturbe and Rinaldo*, 1997; *Tejedor et al.*, 2015a,b; *Smart and Moruzzi*, 1972]. Generally-speaking, three types of channel networks exist [*Kleinhans*, 2010; *Limaye*, 2017]: (1) systems where flow paths are generally convergent, such as tributary stream networks with more frequent confluences than bifurcations; (2) systems with divergent characteristics like deltas and alluvial fans with more frequent bifurcations than confluences, and (3) chain-like systems such as braided rivers, anastomosing rivers and estuaries with similar frequencies of bifurcations and confluences (Fig. 1). While methods relying on surface gradients are generally successful at extracting channel networks from topography in convergent systems [*Tarboton and Ames*, 2001; *Passalacqua et al.*, 2015], the extraction of chain-like, divergent and bifurcating channel networks from topographic data remains an open challenge. While progress has been made [e.g., *Limaye*, 2017; *van Dijk et al.*, 2019], there is a need for an objective, algorithmic method for the extraction and analysis of multi-thread channel network topology and geometry from topographic data. Consequently, we do not know and cannot quantify in what aspects the channel networks of braided rivers, deltas and multi-channel estuaries differ beyond the obvious. This paper aims to fill that gap. Results from earlier versions of this framework have been presented in *van Dijk et al.* [2019].

Channel networks are often identified from either digital elevation models (DEMs) [*Fagherazzi et al.*, 1999; *Montgomery and Dietrich*, 1989; *Passalacqua et al.*, 2015; *Tarboton et al.*, 1991; *Tarboton*, 1997] or imagery [*Dillabaugh et al.*, 2002; *Edmonds et al.*, 2011; *Isikdogan et al.*, 2015, 2017; *Marra et al.*, 2014; *Passalacqua et al.*, 2013; *Pavelsky and Smith*, 2008]. Classically, methods for extracting channel networks from DEMs have relied on the concepts of steepest descent, flow direction assignment, and the delineation of channels based on flow accumulation [e.g., *Lacroix et al.*, 2002; *Pelletier*, 204; *Shelef and Hilley*, 2013; *Tarboton et al.*, 1991; *Tarboton*, 1997; *Tarboton and Ames*, 2001]. With the advent of high-resolution topography data from lidar [*Tarolli*, 2014], more sophisticated channel network identification algorithms for high-resolution data have emerged in recent years [*Lashermes et al.*, 2007; *Passalacqua et al.*, 2010; *Pelletier*, 2013; *Sangireddy et al.*, 2016a]. Methods relying on surface gradients and flow accumulation are generally effective in convergent systems like tributary networks, but fail in multi-threaded channel networks that bifurcate and recombine. Important reasons are that the condition of flow following the path of steepest descent is violated, bed steps with negative slopes are present at bifurcations and confluences, and channels may diverge over shallow bars, shoals and sills which renders their recognition with local path-seeking algorithms impractical. These methods are also sensitive to noise and local highs. An alternative strategy for delineating channel networks from DEMs is through the use of hydrodynamic modeling to track inundation patterns. This strategy can robustly capture bifurcations and convergences in a complicated system [e.g., *Limaye*, 2017], but currently does not yield a network topology nor does it identify the channel thalweg, while it is computationally expensive and sensitive to assumptions in boundary conditions and hydraulic resistance.

The identification of channels from imagery often requires the use of spectral thresholding or classification schemes to distinguish between water and land features, followed by mapping of channels from the resulting image in both the experimental [e.g., *Ashworth et al.*, 2006; *Wickert et al.*, 2013] and natural settings [e.g., *Edmonds et al.*, 2011; *Marra et al.*, 2014; *Passalacqua et al.*, 2013; *Welber et al.*, 2012]. In numerical models generating multi-thread systems, thresholds are often used to distinguish channels from bars and floodplains [e.g., *Schuurman and Kleinhans*, 2015; *Liang*

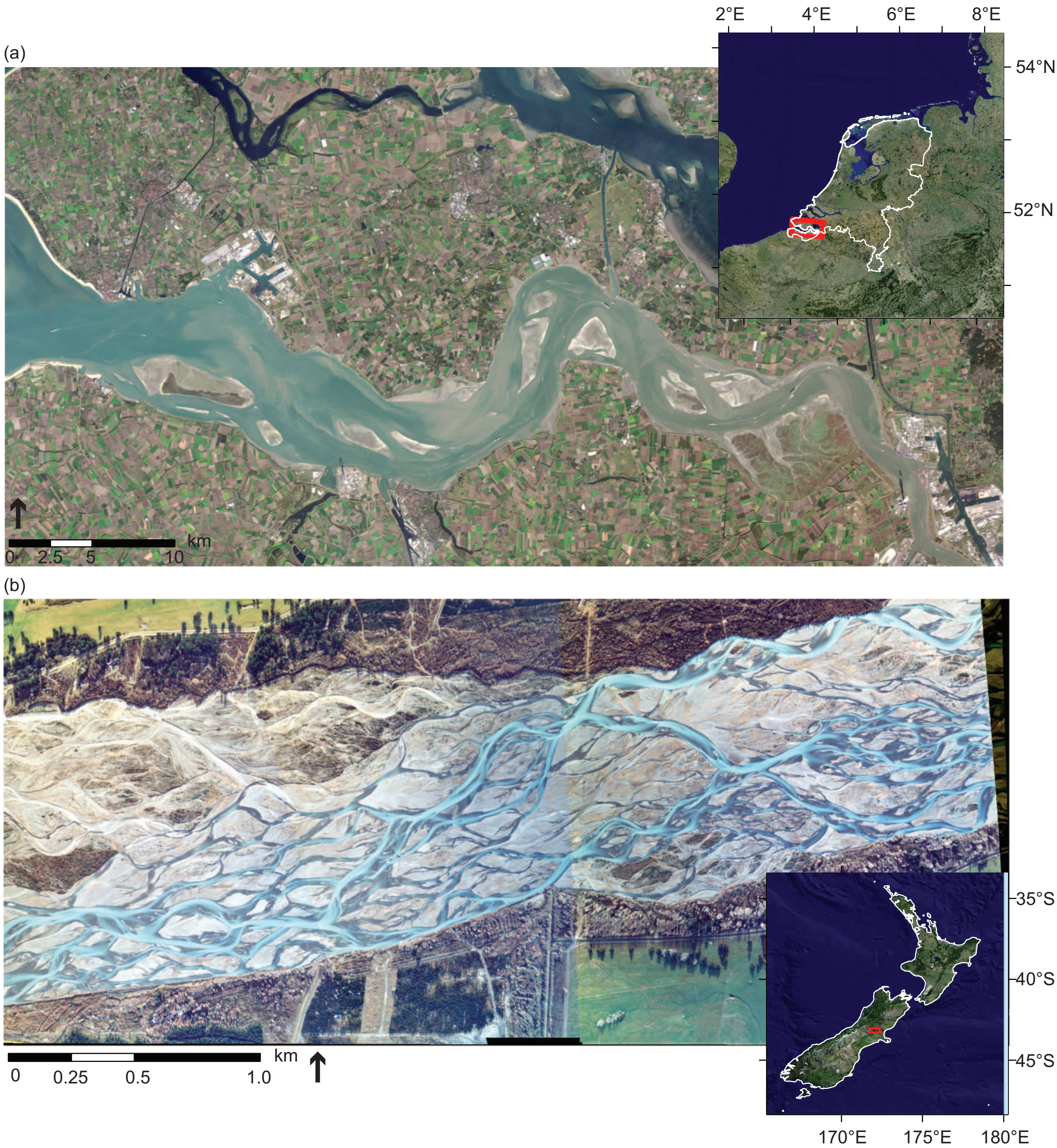

Figure 1. Examples of multichannel networks with similar frequencies of bifurcations and confluences: (a) The Western Scheldt Estuary in the Netherlands (LANDSAT 8 image downloaded from USGS Earth Explorer at https://earthexplorer.usgs.gov/) and (b) the Waimakariri River, a braided river north of Christchurch in New Zealand (imagery from *Hicks et al.* [2007]). Inset images are composite satellite images produced by MDA Information Systems.

et al., 2016]. More sophisticated algorithms exist [*Dillabaugh et al.*, 2002; *Isikdogan et al.*, 2015, 2017; *Pavelsky and Smith*, 2008], but current methodologies are sensitive to local bed elevation increases and still struggle to maintain channel network connectivity at bifurcations and confluences [*Isikdogan et al.*, 2015].

Channel planform geometry is influenced by a plethora of environmental factors including water discharge [*Leopold and Wolman*, 1957; *Van den Berg*, 1995], sediment composition and transport [*Church*, 2006; *Orton and Reading*, 1993; *Braat et al.*, 2017], lithology [*Townend*, 2012; *Nittrouer et al.*, 2011], bank strength and vegetation [*Millar*, 2000; *Tal and Paola*, 2010; *Tal et al.*, 2004; *Vandenbruwaene et al.*, 2011], climate [*Phillips and Jerolmack*, 2016], receiving basin characteristics like tides and waves [*Galloway*, 1975; *Jerolmack and Swenson*, 2007; *Rossi et al.*, 2016; *Geleynse et al.*, 2011; *Nienhuis et al.*, 2018]. Braided rivers have high rates of morphological change, which is due to the abundance of non-cohesive sediment and high stream power [*Kleinhans and van den Berg*, 2011]. The primary requirements for the development of braided river patterns are thought to be the presence of a movable bed and a wide braid plain [*Kleinhans*, 2010; *Kleinhans and van den Berg*, 2011], although modeling work also suggests that bank erosion and boundary condition fluctuations are necessary for maintaining dynamic equilibrium [*Schuurman et al.*, 2013]. Estuarine channel network morphology is shaped by the competition between tidally- and fluvially-driven transport [*van Veen*, 1950; *Robinson*, 1960; *Van der Wegen and Roelvink*, 2012] and sediment composition [*Braat et al.*, 2017]. While subject to different boundary conditions, braided rivers and estuaries can share similar chainlike multichannel networks that bifurcate and recombine at similar frequencies (Fig. 1a,b). Thus, an investigation into the similarities and differences in channel network structures of estuaries and braided rivers may yield insight into the processes affecting their morphologies.

This paper introduces a mathematically rigorous, practical, and noise-insensitive method for extracting multichannel networks from topographic data of rivers and estuaries in reality, models, and experiments in order to analyze the structure and geometry of the channel network. The channel extraction tool, called LowPath, utilizes an algorithm first introduced by *Kleinhans et al.* [2017] that relies on identifying sets of channels that have the lowest path (in terms of elevation) from the source to the sink of the system. This framework can produce a topologically-complete network with geometric attributes using only topographic information. Comparisons are made between estuaries with multiple channels and braided rivers from both nature and morphodynamic numerical models. The output from these analyses yields insight into the processes affecting the morphology of multi-channel systems.

The remainder of this paper is organized as follows. Section 2 provides an overview of the network extraction method, LowPath, and details the location of or modeling setup of four case studies: the Western Scheldt estuary in the Netherlands, Waimakariri River in New Zealand, the braided river model of *Schuurman et al.* [2013], and the multi-channel, bar-built estuary model of *Braat et al.* [2017]. The results of the network extraction are presented in Section 3, followed by results of the topological and geometric analyses performed on the extracted channel networks (Section 4). The implications of the results are discussed in Section 5, along with an exploration of the role of scale in network delineation from topographic surfaces. Section 5 also contains notes for future avenues of research. The conclusions are stated in Section 6.

2 Background and Methods

2.1 A primer on network terminology

A network is a mathematical representation of a set of objects and the connections among those objects [*Newman*, 2003]. Networks are made up of two types of elements, *links* and *nodes*, where *links* delineate how *nodes* are connected to each other. The mathematical representation of the interconnectedness in a network is called the network *topology*, which can be represented by an adjacency matrix where rows and columns represent nodes and the entries of the matrix represent the links between the nodes. In the case of a braided river or estuary, nodes represent bifurcations, or sometimes polyfurcations, confluences, inlets, and outlets, while links represent channel centerlines or thalwegs (Fig. 2). A path is a sequence of links that connect the starting and ending nodes of the system.

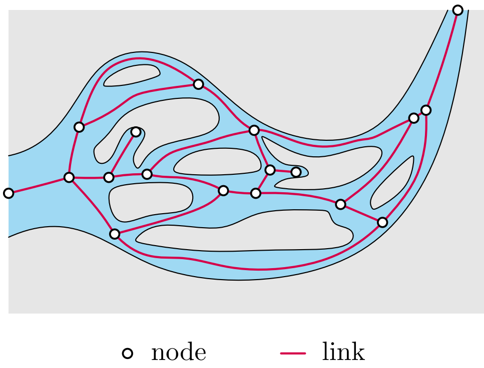

Figure 2. Example of a network for a multichannel system.

2.2 Theory

A common challenge in geomorphology and hydrology is delineating a channel network from a DEM. Objectively doing so in a dataset containing many bifurcations and confluences has proved elusive, due to complications such as longitudinal variations in channel depth and slope, and violations of steepest descent principles, among others. Recently, however, a mathematically-rigorous framework was introduced by *Kleinhans et al.* [2017] for the extraction of multi-threaded channel networks from topographic surfaces. This method is an effective data reduction method for complete DEMs without elevation-thresholding or binarization, that is especially suitable for calculations of bed elevation and other properties on channels. Additionally, its application is not limited to multichannel systems, as a single channel network can also be objectively identified. Whilst not pursued here, the delineation of channels also implies that the method can be used to identify bars at a range of scales. Here we qualitatively describe the theory behind the operation of the LowPath algorithm at a level required to understand the results presented below. A detailed description of the mathematical principles underlying the method, as well as mathematical proofs, can be found in the work of *Kleinhans et al.* [2017].

The algorithm takes as input a DEM of the bed level of a braided river or estuary. Because it uses only the elevation of the bed level, the generated network is independent of the water level. However, the algorithm could in principle be applied to other maps, including depth or velocity fields. To construct the network, the algorithm computes so-called *lowest paths* through the DEM. A lowest path between two points is a path that does not traverse any elevations higher than those necessary to connect the two points. To help in constructing lowest paths, the algorithm first computes a *descending Morse-Smale complex* (MSC) [*Edelsbrunner et al.*, 2001; *Kleinhans et al.*, 2017; *Shivashankar et al.*, 2012]. The MSC of a DEM is a topological complex that describes the structural elements of the terrain. It contains the local minima, maxima and saddle points (points that are a local minimum in one direction while being a

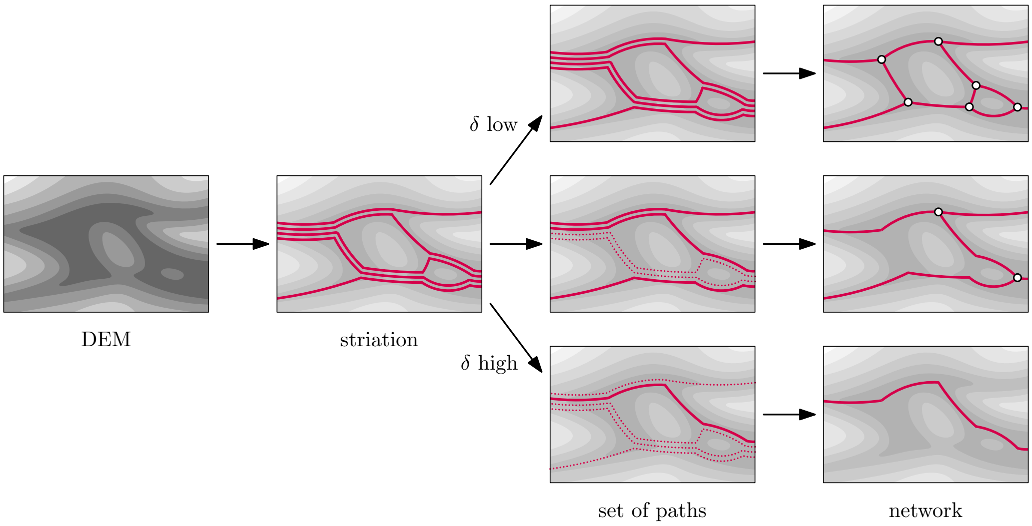

Figure 3. A qualitative depiction of how LowPath determines the channel network. First, from the river bed DEM, the striation is computed (left). Consequently a set of sufficiently different paths is found (center; here depicted for three values of δ), which form the final network (right).

local maximum in the other), and steepest-descent paths (called *MS-links*) from saddle points towards minima. *Kleinhans et al.* [2017] showed that lowest paths always traverse the MS-links of the MSC, which means that lowest paths can be computed efficiently.

Instead of just one single lowest path, the algorithm needs to compute a complete set of paths that together form the entire channel network. To achieve this, the algorithm sequentially finds lowest paths in parts of the DEM. More precisely, after the first lowest path π is found, the DEM is split around π into two parts. Then the lowest paths in those two parts of the river are found, the DEM is split around these paths, and so on. (In fact, the splitting procedure is somewhat more complicated, to avoid issues if π does not entirely lie on the boundary of its part of the DEM. We refer to *Kleinhans et al.* [2017] for more details.) All the paths found in this fashion form an ordered set of non-crossing paths, called a *striation* (see Fig. 3 left).

In general the striation contains a large number of paths. Since the resolution of a DEM typically is such that channels are several to many grid cells wide, it may contain several paths within the same channel, which would be undesirable in the network. To alleviate this, we need a way to determine for two striation paths whether they are 'sufficiently different' to form two separate channels. Then, the algorithm picks a subset of the striation paths, which are all sufficiently different, to obtain the network (see Fig. 3 center and right).

To decide if two paths are sufficiently different, we consider the volume of sediment that separates them: the larger the volume, the more different the channels are. The sediment volume is a morphologically meaningful way to distinguish channels, because volume is related to the morphological work required to cut bars and merge channels [e.g. *Kleinhans*, 2005]. The volume is measured using a so-called *sand function*, which is defined mathematically as the minimum volume above a descending isotopy between the two paths. Informally speaking, this means measuring the volume of sediment that obstructs one path from sliding downhill towards the other path. Then we define two paths to be sufficiently different, and allow them to be in the network together, if and only if the volume is larger than some threshold δ. Lowering δ means that channels with smaller bars in between are distinguished as sufficiently different channels. Higher δ values on the other hand require larger bars between channels for them to be distinguished as sufficiently different. Therefore, by generating several networks with different values of δ, channels across a range of scales are identified (Fig. 3).

In the resulting network, the existence of a path can be affected by the existence of another path in seaward (downstream) or landward (upstream) direction. This is the result of the threshold δ being reached by the summation of several bar deposits between paths. This means that the threshold volume could in principle be reached by the volume at one end of the system alone depending on the order of the sorted paths. Therefore, for example, two paths in the network may be close to one another in one section of the system, simply because they are separated by a large volume of sediment in another section.

2.3 Workflow

The general workflow, including pre- and post-processing steps, necessary to generate a network from a DEM is briefly described. The three main steps are the preparation of the DEM, application of the LowPath algorithm as described in the previous section, and the assignment of topographic and geometric information to links and nodes.

We used an extended version of the implementation used in the original paper by *Kleinhans et al.* [2017]. As input, this implementation requires only a topographic surface (image file or text file) to output the set of lowest paths and network nodes. Geometric properties of the DEM must be specified, including the horizontal resolutions of the grid cells in the x- and y-directions. Only rectangular grids are accepted, but the grid cells do not need to be square. The elevation range (i.e., the minimum and maximum elevations) of the DEM must be included for the image-based input to be able to properly calculate volumes, because this is the best available estimate of the reworkable sand body that is assumed in the sand function. To ensure that only the river bed itself is analyzed for network paths, and not for example the surrounding floodplain, as a preprocessing step the user is able to mask grid cells that they do not want included in the calculation. The user must also specify the δ value or range of values.

As described in the previous section, LowPath generates a network consisting of a set of sufficiently different paths. How many paths are included in the network is determined by the selection of δ. At the higher end of the δ spectrum (i.e., large volumes of sediment) only a single path is extracted. This is the overall lowest path that traverses the riverbed. As δ decreases, the number of paths extracted generally increases, because the volume between adjacent paths needed to identify channels as sufficiently different is decreasing. Eventually, as δ nears zero, the returned network contains all striation paths. In other words, varying the parameter δ allows us to obtain networks across a wide range of scales.

In this paper, we want to classify individual channels in the river based on their importance. Because the number of channels increases when δ decreases, a measure of the importance of a channel is the highest δ value at which that channel still appears in the network. To compute these δ values per channel, we first perform the network computation for a wide range of δ values, say, $\delta_1 > \delta_2 > \ldots > \delta_k$. This results in k networks, called differential networks, which we then combine into a single composite network (Fig. 4). In every network computation, the striation is identical, because the computation of the striation is independent of the value of δ. However, the set of paths selected for inclusion in the network differs. Generally, paths included in the network for δ_i will also be included for δ_{i-1}, which leads to significant path overlap when condensing the sets of paths into the composite network. This issue is rectified by a series of post-processing steps as follows:

1. Channels that are included for multiple δ scales are filtered such that only the largest δ scale at which the channel was detected remains (Fig. 4c). Thus the paths detected by the LowPath algorithm have been converted to network links with starting and ending nodes.
2. In some cases, paths at the same scale overlap at certain points in space, which may cause connectivity issues following step 1. To maintain connectivity, links may be split into smaller sections and nodes are added at their endpoints.
3. The channel network is then further segregated into smaller differential networks that detail the nodes and links found at each δ scale (Fig. 4d-g).

After these post-processing steps, data detailing the coordinates, scales, and the topology of links and nodes is available. An adjacency matrix A is generated for the composite network and the δ differential as a representation of the topology. Geometric information can also be assigned to the links and nodes, such as elevation, channel slope, channel length, or sinuosity.

2.4 Analysis

In this paper, we use LowPath and the previously-described processing methodology to extract channel network and geometric information from topographic data for both estuaries and braided rivers for analysis and comparison. Both the differential networks and the complete composite network for each dataset are analyzed. Four datasets are used: a set of DEMs resulting for the morphodynamic modeling of a braided river [*Schuurman et al.*, 2013], a lidar DEM of the Waimakariri River in New Zealand [*Hicks et al.*, 2007], a set of DEMs from a morphodynamic model of estuary development [*Braat et al.*, 2017], and a DEM of the Western Scheldt estuary in The Netherlands [*van Dijk et al.*, 2018, 2019]. In an earlier paper the original implementation of the algorithm was also demonstrated to work for experiments [*Kleinhans et al.*, 2017].

A range of statistical metrics have classically been used to describe channel network topology and geometry after the channel network has been extracted. Previous research has largely focused on planform geometries of channels and bars for characterizing the geometry of multi-thread channels [e.g., *Limaye*, 2017; *Leuven et al.*, 2016, 2017, 2018, and add others]. Braiding index or intensity is another commonly-utilized metric that quantifies the number of active channels across the width of the channel belt, which we forgo in this paper because it has been addressed and quantified in other studies [e.g., *Howard et al.*, 1970; *Germanoski and Schumm*, 1993; *Egozi and Ashmore*, 2008; *Crosato and Mosselman*, 2009; *Bertoldi et al.*, 2009; *Kleinhans and van den Berg*, 2011; *Schuurman et al.*, 2013; *Leuven et al.*, 2016, 2017; *Braat et al.*, 2017; *Leuven et al.*, 2018]. *Redolfi et al.* [2016] identified the utility of using reach-scale bed elevation distributions in braided rivers to inform morphological trajectories. However, there lacks information regarding bed-elevation distributions within the channel network itself, likely due to limitations in network extraction methodologies. This paper focuses on describing multi-thread channel networks as a function of channel bed elevation distributions across different morphologically-informed scales (i.e., the sand function scale δ).

For each dataset, we analyze the structure of the network at a range of sand function scales (δ), measure the distribution of elevations along each link in the network, measure the number of nodes and links at each scale, and calculate the distribution

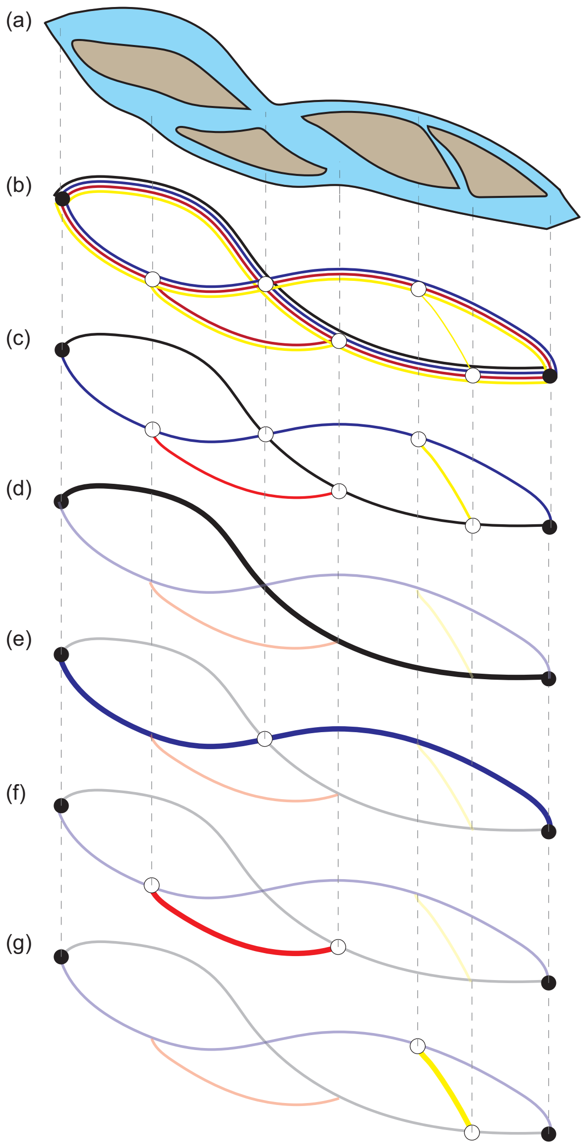

332 **Figure 4.** Breakdown of the steps necessary to create a network from topographic data (a)
333 using LowPath and post-processing tools. (b) Channel centerlines and locations of overlap or
334 nodes (circles) are output from LowPath across a range of sand function scales (from smallest
335 to largest scale: yellow, red, blue, black). Adjacent lines depict overlap of channels extracted at
336 different scales. The smallest scale channels are detected everywhere that a larger scale channel is
337 also detected, leading to relatively large/deep channels being detected at a large number of scales
338 (depicted by adjacent links). (c) Overlapping channels are systematically removed such that each
339 detected channel centerline belongs to a single sand function scale. (d-g) Finally, the network is
340 segmented into smaller sub-networks that depict the network associated with a single sand func-
341 tion scale. Doing so allows channel geometries to be assigned to the network independent of the
342 influence from other scales.

Table 1. Summary of the sand function scales for each data set

Data Set	δ range (m^3)	grid resolution (m × m)	est. avg. braid belt width (m)
Braided River	$3.98{\times}10^2$ – $3.98{\times}10^9$	200 × 80	3280
Waimakariri	$1.09{\times}10^2$ – $1.09{\times}10^7$	8 × 8	1050
Estuary Model	$1.20{\times}10^2$ – $1.20{\times}10^8$	50 × 50	2590 (mouth) - 250 (upstream)
Western Scheldt	$1.20{\times}10^2$ – $1.20{\times}10^9$	100 × 100	5660 (mouth) - 2500 (upstream)

of link lengths for each scale. The elevation distributions are calculated by extracting the elevation in the DEM cell at each coordinate for every link in the network. Cells located at channel confluences and bifurcations are excluded, because these points may bias the results when partitioning the data among the various δ scales. For example, if a small, narrow, and shallow secondary chute channel meets the deep main channel, the depth at their confluence may significantly skew the depth distribution of the smaller channel, since the main channel is significantly deeper. Therefore, elevations at these coordinates are excluded when calculating elevation distributions.

Each case study is run at δ scales ranging several orders of magnitude (Table 1). The range of scales is determined by the geometric characteristics of each individual system (e.g., elevation relief, planform extent, system slope, etc.). Since the four case studies chosen range considerably in size, the ranges of δ values are different for each system. However, δ values were selected to ensure that the largest δ scale produced a single main channel and a simple sensitivity analysis was performed to determine the minimum scale at which this channel is manifested. After the largest δ was determined, δ values were sequentially decreased by one order of magnitude until reaching a δ scale that was on the same order as the horizontal grid cell size. Values of δ below this value are physically unrealistic, because channels cannot be detected at finer resolution than one pixel. In the results section, δ is represented qualitatively (from high to low values) rather than quantitatively (actual δ values) for convenience when comparing data sets of significantly different size (see Table 1).

3 Channel network extraction

The network structure and geometries are presented for the four datasets discussed in Section 2.4. The LowPath algorithm produces channel networks that follow the lowest paths through the topographic surface. Therefore, the extracted network links represent channel thalwegs (the deepest portion of the channel) for the full extent of each channel. For the modeling studies, a representative timestep was chosen for analysis based on the changes to the number of nodes and networks likes across δ scales through time (e.g., Fig. 5). For example, the braided river model of *Schuurman et al.* [2013] was determined to be at a dynamic equilibrium state at around timestep 180 (Fig. 5), which is equivalent to about 12 months of morphological development under permanent bankfull flow conditions. The timestep was selected because it marked the beginning of a relatively stable period for the number of nodes and links extracted. The same procedure was performed for the estuary model.

Networks are decomposed into differential networks (Fig. 6) to isolate the effects of scale on network structure. We use topography from the braided river model of *Schuurman et al.* [2013] to illustrate these results in Fig. 6. At the highest sand function scale (δ), there is one (and only one) lowest path that traverses the landscape from the upstream to downstream boundary (Fig. 6). The single link detected at

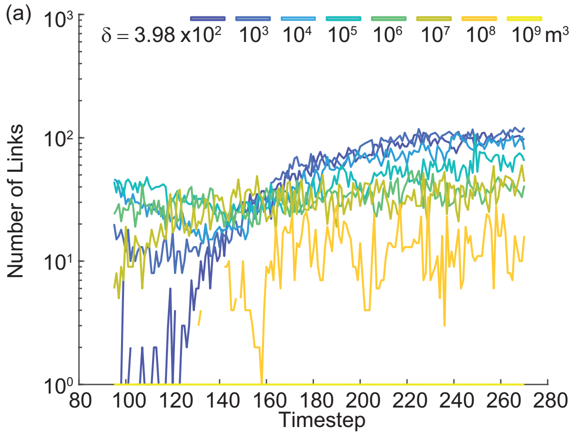

Figure 5. Network change over time for the braided river model of *Schuurman et al.* [2013]. The channel network at timestep 180 was chosen for analysis in Fig. 6 because it represents the beginning of a relatively steady period of number of nodes and links at each δ scale.

the largest δ scale is representative of the "main" channel of the system. Decreases in δ tend to cause a greater number of channels to be detected, and those channels appear to become shorter in length relative to larger scales (Fig. 6). In the braided river model (Fig. 6), the link detected at the highest δ value (i.e., the main channel) follows an uninterrupted, sinuous path from the inlet to the outlet. The links with the second-highest δ value follows a largely similar pattern, but interruptions in the continuity of the links result generally from where these links connect with the highest δ scale link. Discontinuities among the links at scale δ are often due to intersections with links at scales greater than the δ of interest.

The spatial arrangement of channels in the two estuarine examples differs from the two braided river systems. Both the channel network of the braided river model (Fig. 6) and the channel network of the Waimakariri River (Fig. 7a) exhibit a high link density relative to their estuarine counterparts: the Western Scheldt (Fig. 7b) and the estuary model (Fig. 7c). The estuarine systems tend to have relatively large portions of the channel belt where no links were detected, which is indicative of relatively flat, un-channelized portions of the landscape. These regions vary in size and position within the landscape. By contrast, the links of the braided river systems are uniformly represented throughout the landscape and the un-channelized portions of the landscape have a relatively uniform size and spacing. There does not appear to be a clear spatial clustering associated with the δ value at which channels are detected in the braided river case studies (Figs. 6 and 7a), but there appear to be zones of high density of small δ scale channels with bar complexes in the estuarine example of the Western Scheldt (Fig. 7b). This behavior is difficult to identify within the estuary model (Fig. 7c) because relatively few channels are detected across scales, and the resolution of the numerical model is lower.

Channel bifurcations and confluences are identified during network extractions, and nodes are placed where links bifurcate or join. LowPath maintains the connectivity of these network elements, such that topological information is not lost. The geometric information of bifurcations and confluences is nested within both the elevations at which links and nodes are extracted, but is also manifested in the δ scales of bifurcating or joining links. Notably, most bifurcations involve branches that are identified at different δ values, indicating that the geometry of the two branch channels and the deposited material separating them differ. This indicates that many of the identified

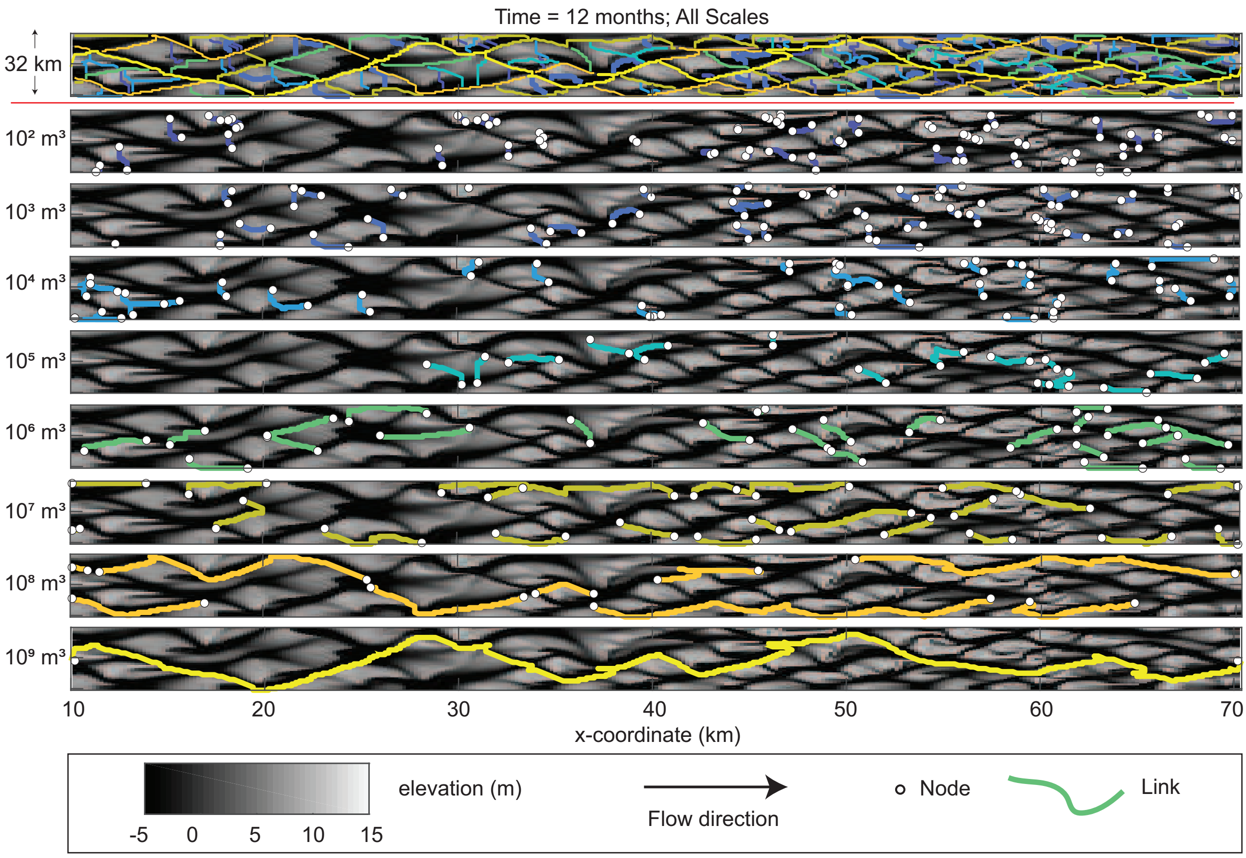

Figure 6. Summary of a multi-scale network in the modeled braided river dataset. The top panel shows the channel network for a range of scales (network nodes are excluded for visualization clarity). The colors of the channels indicate the sand function scale. The following panels show the channel network partitioned by volumetric sand function scale. At lower sand function scales, channels are relatively short and are often oriented perpendicular to the flow direction. Channels become longer and more parallel to the mean flow direction with increasing scale. The elevation scale is truncated at the lower end for visualization and to match the representation in *Schuurman et al.* [2013].

bifurcations are not morphologically-symmetrical (Fig. 7). The tendency of bifurcating channels to be at different δ scales can be seen by decomposing the channel network into separate layers based on δ scale (e.g., Fig. 6).

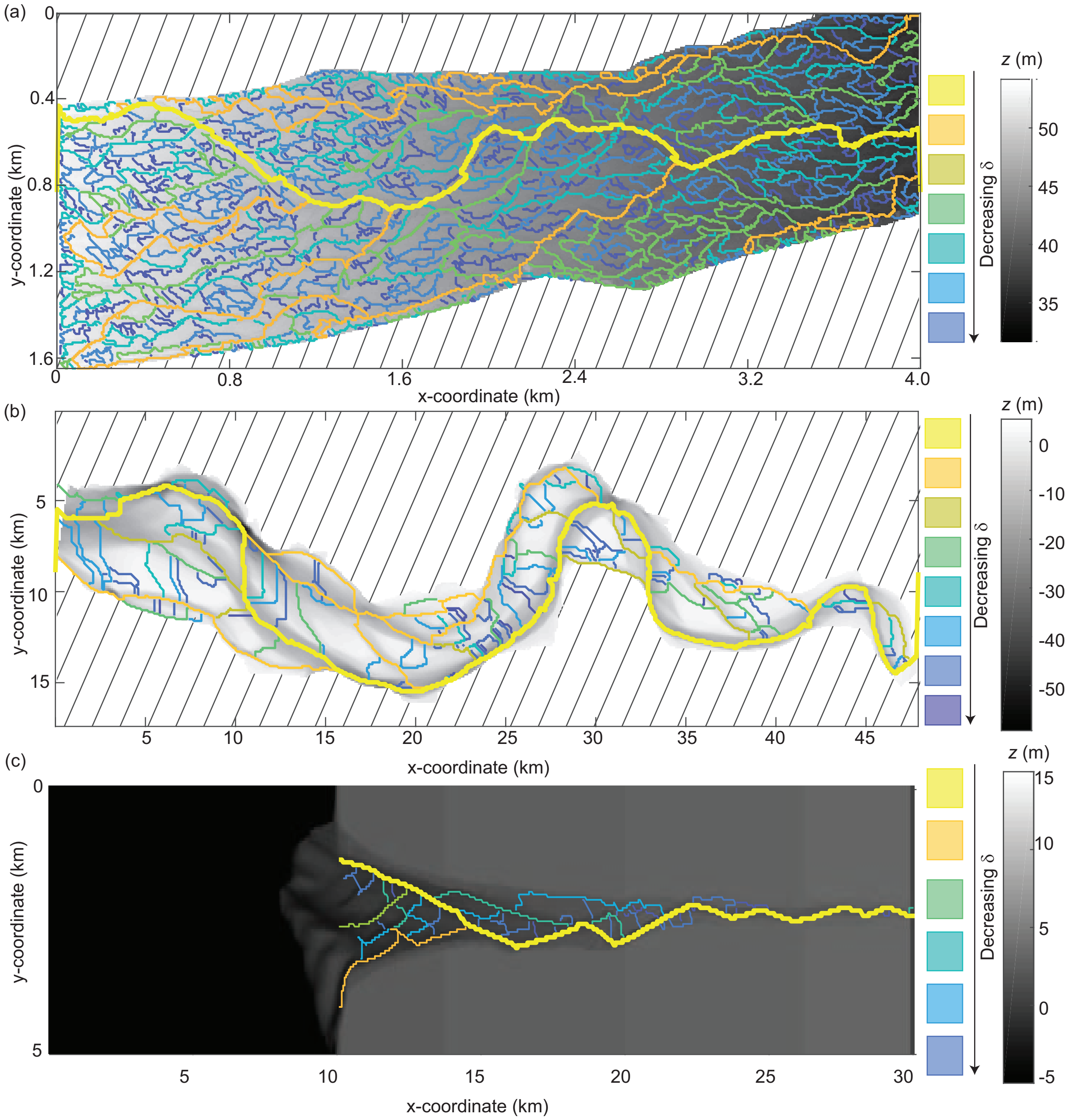

Figure 7. Network extractions for (a) the Waimakariri River (New Zealand), (b) the Western Scheldt estuary (Netherlands), and (c) the results of an estuarine morphodynamics model [*Braat et al.*, 2017]. Note the scale exaggeration of the y-coordinate of (c) done for visualization purposes.. The hashed lines represent areas outside the domain.

Link length decreases with decreasing δ scale. The relatively-deep and -wide main channel traverses the extent of the system and is thus significantly longer than those smaller, narrower channels that develop on top of bar surfaces (Fig. 6). In between these two extremes, there is a general behavior of increasing link length with increasing δ. This result is expected, since δ is representative of the relative spatial scale of the channel, and larger channels are less likely to be intersected by channels of equal or larger size, and therefore have a tendency to be detected as relatively-long and continuous links. This phenomenon holds for both the all of the cases studied.

4 Topology and geometry

This section presents analyses performed on the extracted networks from Section 3 and identifies several topological and geometric characteristics of the studied multi-channel systems. The goals of these analyses are to understand how channel network structure varies among different systems and to analyze the extent to which scale influences the internal organization of these channel networks. We present results for the four case studies for which channel networks were extracted with LowPath (Figs. 6 and 7).

The number of links in the composite network detected in a given δ scale generally decreases as the scale fraction value increases for each case study (Fig. 8a). The Waimakariri has the most links across scales, which is likely due to the relatively high resolution of the topography relative to the width of the braid belt. The estuary model has generally the least number of channel links for a given δ value due to the low number of channels detected. The channel network extracted for the Waimakariri has significantly more links than that of the braided river model (noted as BR model in Fig. 8a) and the same is true for the Western Scheldt versus the estuary model (Fig. 8a). The difference in number of links at a given δ value between natural and model systems is about one order of magnitude.

Within differential networks, the number of nodes detected at a given scale is generally twice the number of links detected at that scale, since a link has a starting and ending node. Multiple links originating from or ending on shared nodes may decrease this total. The inverse relation between node number and δ does exhibit some variability and there are examples where increasing δ values do not cause a decrease in node number. This is likely due to the inherent variability in natural systems and the choice of threshold for δ values. At the upper threshold of δ values there are always two nodes detected for the single "main" channel.

The length of each link in the composite network is calculated from the geometric information provided by the topographic surface. For each link i at a given scale $\delta = j$, the normalized length is calculated as:

$$\bar{L}_{\delta=j,i} = \frac{L_{\delta=j,i}}{L_{LP}} \tag{1}$$

where L is the length of the link denoted with a subscript i, the subscript j is the delta scale of interest, and L_{LP} is the length of the single link extracted at the maximum δ scale (i.e., the lowest path). Likewise, we introduce another normalization to account for the difference in δ thresholds among the case studies. For each case site, the Scale Fraction, is calculated as the scale of interest δ, i divided by the largest sand fraction scale δ_{max}. The values for both Scale Fraction and $\bar{L}_{\delta=j,i}$ range between 0 and 1. Performing these normalizations allows for systems of much different spatial scales to be quantitatively compared.

The normalized link length is positively related with scale fraction and appears to follow power-law increase behavior (Fig. 8b). The exponent on the power relation

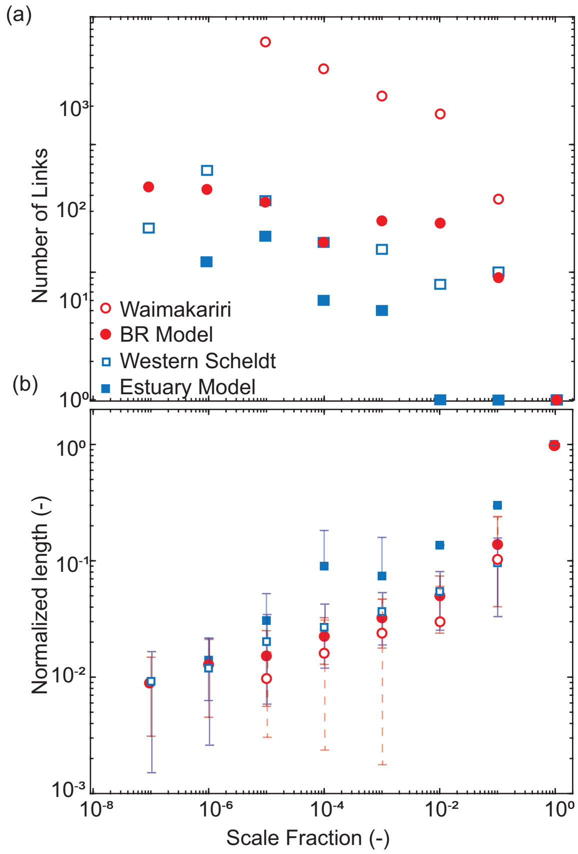

Figure 8. (a) The number of links per scale fraction. (b) The normalized length for links for each data set across the range of delta scales. The sand fraction scales are presented as fractions of the largest scale. The symbols represent the medians of the normalized link length distributions and the error bars represent the ranges. The mean length of links generally increases with increasing δ. The data appears to follow a power-law decay (see text for details).

is 0.23 for the braided river model, 0.27 for the estuary model, 0.24 for the Western Scheldt, and 0.35 for the Waimakariri River. The magnitude of normalized length is mostly similar among the case studies throughout the range of scale fractions considered. However, the estuary model normalized length tends to consistently plot at higher values than those of the other cases, especially at the scale fraction of 10^{-4}, where the normalized length for the estuary model is nearly an order of magnitude greater than the other three cases.

The frequency distributions of slope-corrected channel bed elevations for the composite network of each case study are displayed in Fig. 9. Depth distributions are constructed by extracting depth values for each pixel that lies under a link at a given sand function scale. The depth distributions are partitioned into contributions from each δ scale tested to determine how channel bed elevation changes with scale (those classifications are presented qualitatively in Fig. 9). In the Waimakariri River channel network, elevations associated with small δ values are generally higher than those associated with larger δ values (Fig. 9a). In the Waimakariri River example, this transition from higher to lower elevations as δ increases is fairly gradual which results in a fairly symmetrical, unimodal distribution shape. Additionally, in the Waimakariri River, there are a higher frequency of elevations associated with small δ values. This is due to the large number of channels detected at small δ scales present in the Waimakariri River channel network. Higher δ scales have relatively few low elevation values. This pattern of sequentially decreasing elevation with scale is clear for Waimakariri River channel network.

The slope-corrected elevation frequency distribution of the braided river model channel network exhibits the behavior of decreasing elevations as δ increases (Fig. 9b), but the pattern of decreasing frequency in elevation counts from low to high δ values is not present as it is in the Waimakariri River system (Fig. 9a). While the overall shape of the elevation distribution appears to be bimodal, the distributions of elevation at each individual δ scale is unimodal. The largest δ scale occupies a large portion of the overall network distribution, which suggests that the main channel is relatively long compared to the cumulative length of channels detected at small scales. However, like the Waimakariri River channel network, the links associated with large δ values are found at lower elevations than those identified at small δ values.

The channel network elevation distributions for the Western Scheldt and the estuary model display different behavior. For the Western Scheldt, the channel network elevation distribution follows a similar pattern of low elevation for high δ values and there is a stark increase in elevation frequency at the largest δ scale around an elevation of $z = -20$m (Fig. 9c), which is likely due to channel bed maintenance through dredging activities in the estuary. There is also a fairly wide range of elevations at which the largest δ scale link exists. The frequency of elevations is fairly uniform across smaller δ scales in the Western Scheldt. In the estuary model, the elevation distribution for the highest δ scale is bimodal, which is unique among the cases studied (Fig. 9d). Additionally, the second highest δ value contains some links, albeit at a very low frequency, with the lowest elevation values around $z = -5$m, which again breaks with the general trend observed in the other case studies.

5 Discussion

5.1 Comparison among systems

The novelty of the presented analyses is the combination of a new network extraction tool for bathymetric data and the objective comparison between network topology and morphology of fluvial and tidal systems and of field data and numerical modeling.

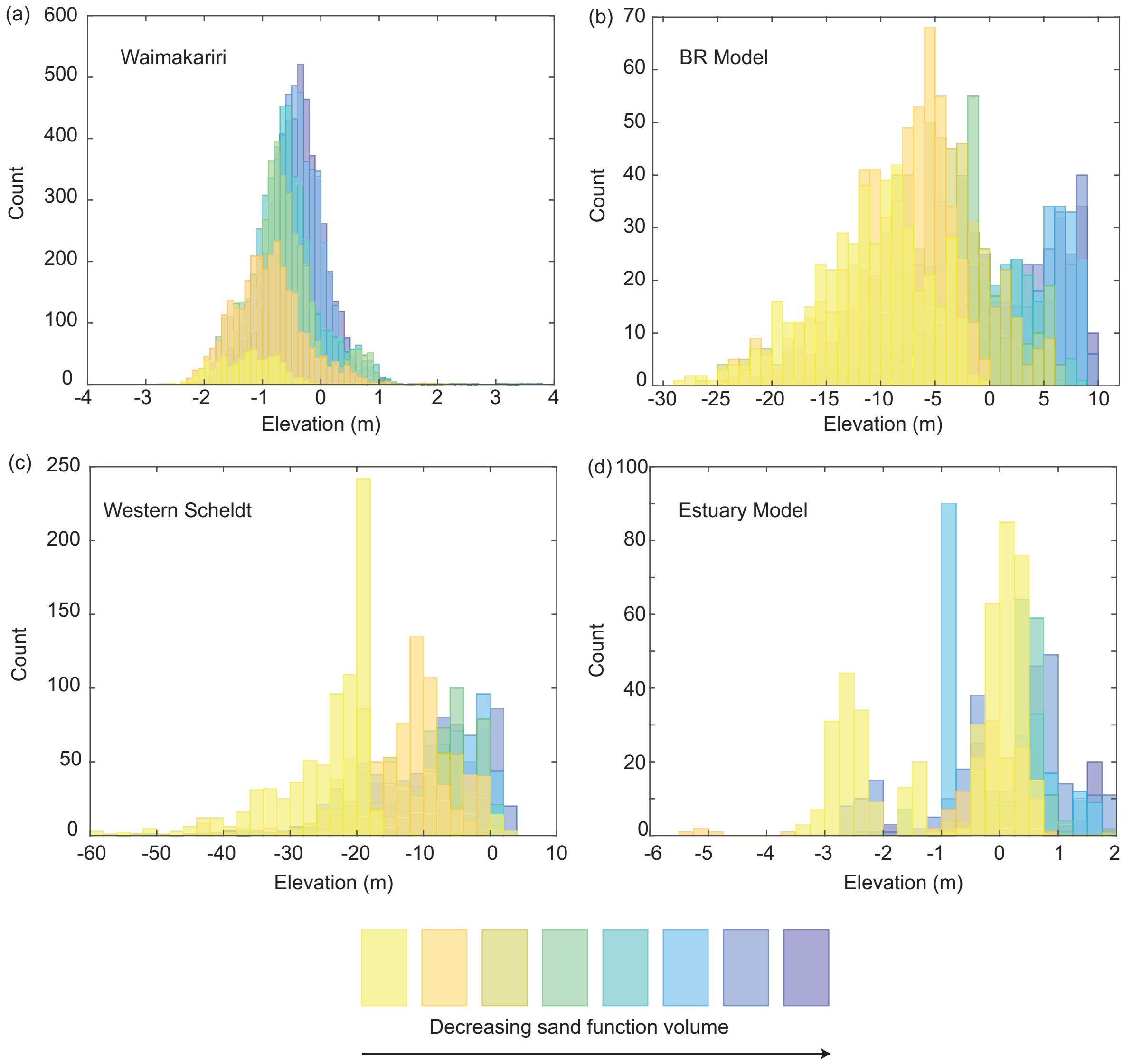

Figure 9. Comparison among the depth distributions across sand function scales for each case study. The elevation values have been corrected for system slope, if necessary.

Our results indicate that there are some quantitative similarities between the structure of braided rivers and estuaries for the cases examined in this text.

Visual inspection of our results indicate that the scales of the two channels downstream of a bifurcation are often not the same in the cases studied (see Figs. 6 & 7). This result seems to align with the generally-accepted consensus that morphodynamically-stable bifurcations must exhibit asymmetrical partitioning of water and sediment fluxes due to geometric asymmetries between the bifurcate channels [*Bolla Pittaluga et al.*, 2003; *Zolezzi et al.*, 2006; *Kleinhans et al.*, 2007, 2008, 2013]. It is reasonable to argue that the geometrical asymmetry associated with the differences in geometry between the bifurcate channels is directly related to the volume of deposited sediment (i.e. channel bar) separating the two channels. Though the discrepancy in scale between bifurcate channels seems to coincide with the literature on bifurcation geometry, the results presented here may be influenced by the calculation of δ within LowPath. In an symmetrical bifurcation, LowPath will still slightly assign different δ values to the bifurcate channels. In our analysis, we selected a range of δ values at intervals of one order of magnitude to assign scales to channels. This large interval dampens the biasing effects of the LowPath algorithm and increases the likelihood that scale differences are due to geometric discrepancies among channels rather than systematic bias.

The division of channel segments into a range of scales with the physically meaningful unit of sediment volume allows for scaling analysis. Scale invariance and power-laws are often used in geomorphology in the search for mechanisms describing system self-organization and scaling [*Dodds and Rothman*, 2000; *Kleinhans et al.*, 2005]. In network analysis, a scale-free network is one whose degree (i.e., the number of connections each node has with other nodes) distribution follows a power-law distribution with an exponent between -2 and -3 [*Albert and Barabási*, 2002]. There is significant spread in the decay of node number as a function of δ, and the slope of the decay does not follow, in general, a power-law decay. Thus, the decrease of nodes as δ scale increases (Fig. 8a) suggests that the configuration of channel networks in estuaries and braided rivers (i.e., the topology) is not scale independent. This may be expected, since channel networks in nature are chain-like [*Marra et al.*, 2014], and the connectivity among channels is limited to those in proximity to one another. This causes the network degree distribution to be fairly uniform: and cannot follow the power-law distribution decay that constitutes a scale-free network. Conversely, the geometry of the networks suggests some scale-invariant properties (Fig. 8b). The normalized length of channel links increases as a power law with an exponent of around 0.30 for all the cases tested. This suggests that the channel networks in estuaries and braided rivers self-organize in a similar fashion, regardless of size of the system.

The length of channels at various scales obviously depends on the overall length scale of the system in question. In Fig. 8b, the length of each network link was normalized by the length of the largest δ scale channel and the normalized length distribution was displayed to compare across systems of different sizes. This metric showed that link length had a rough positive power relation with scale fraction. However, this normalization averages out the effect of the total number of links detected at a given δ scale, which can vary significantly among systems (Figs. 6,7). To address this, we introduce the normalized cumulative length per δ scale as

$$\hat{L}_{\delta=j} = \frac{\sum_{i=1}^{i=N} L_{\delta=j,i}}{L_{\delta=max}} \tag{2}$$

where N is the total number of links at scale $\delta = j$. The normalized cumulative lengths of the braided river model, estuary model, and Western Scheldt systems follow a positive power relation with scale fraction (Fig. 10), but has a negative relation for the Waimakariri (Fig. 10). The behavior of the normalized cumulative length scale with scale fraction for the Waimakariri is opposite of the trend presented in Fig. 8b, while both the normalized cumulative length and the normalized length show similar patterns for the three other systems.

We have two alternative hypotheses for the deviation of the Waimakariri network. First, the much longer collective length of smaller channels than the single main channel may point to an issue of topographic grid resolution. The dependence of extracted channel network features, such as drainage density, on DEM resolution has long been established in catchment hydrology [*Garbrech and Mart*, 1994; *Molnar and Julien*, 2000; *Ariza-Villaverde et al.*, 2015; *Sangireddy et al.*, 2016b], and the phenomena simply depends on the ability of the extraction method to recognize channels and it should recognize smaller channels as grid resolution increases. Many small channels were detected for the Waimakariri system compared to the others (Fig. 3), which is likely due to the relatively fine resolution of the Waimakariri lidar used for channel network extraction (Table 1). Because high cumulative length of channels at small scales relative to the length of the main channel. Thus, for high resolution topographies, this result suggests that small scale channels dominate the behavior of the extracted channel network geometry distributions, while systems with lower resolution grids suggest main channel dominance. This may explain the prevalence of bi-modality in the depth distributions (Fig. 9b,c,d) and lack thereof in the depth distribution for the Waimakariri (Fig. 9a). The second hypothesis is that the larger collective length of smaller channels is a system characteristic. The Waimakariri River is much wider and shallower than the other systems, which leads to a higher braiding index. Regardless of system width, there is only one single main channel with a length of the order of the study reach length, but a higher degree of braiding leads to a higher collective channel length at smaller scales. This hypothesis is supported by the observation that the second-largest scale has already a nearly four times larger collective length, and the smallest scales do not become more than a factor two higher than that. The second-largest scale is not affected by the resolution of the lidar, which argues against the resolution hypothesis.

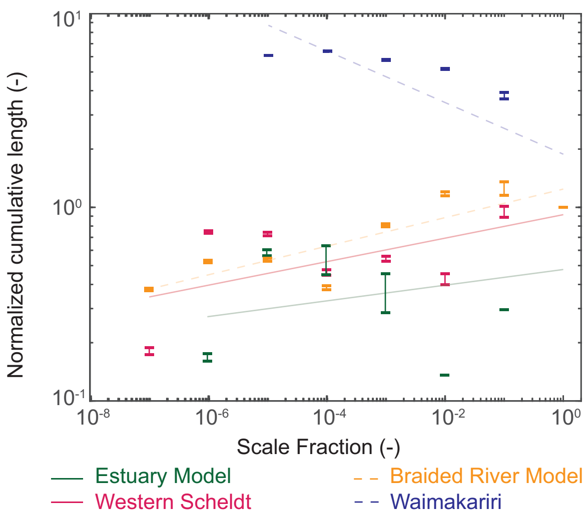

Figure 10. Normalized cumulative length for each tested system with a best fit line included for changes with scale fraction.

The depth distributions (Fig. 9) indicated that braided rivers tend to have more overlap among channel depths across scales (i.e., even large scale channels can be as shallow as small scale ones), but the estuarine systems appeared to have a more bi-model depth distributions suggesting that a single, main channel tends to develop. Several hypotheses explain these trends. First, this is in qualitative agreement with much higher predicted braiding index in river bar theory than tidal bar theory *Leuven et al.* [2016], and also the difference between the modeled and natural braided river is qualitatively expected from their respective channel width-to-depth ratios [*Kleinhans and van den Berg*, 2011]. Another possible cause for the deeper estuarine channel is that the natural, mid-twentieth century channel depth in the Western Scheldt has been increased by several meters [*Verbeek et al.*, 1998], while the secondary and smaller channel depths decreased due to dredging for fairway maintenance as demonstrated by modeling compared to controls without dredging [*van Dijk et al.*, 2019]. A third hypothesis is that morphological models may have a tendency to erode channels and over-steepened the bars. Though the estuary model [*Braat et al.*, 2017] was run with a high bed slope effect parameter that prevents such erosion but also subdues bars and reduces the braiding index [*Baar*, 2019]. While this model exhibits bi-modality in the depth distribution, the relatively small number of channels available for extraction at any given timestep is likely the source of significant temporal variability in depth distributions. On the other hand, the braided river model had a much lower bed slope effect and showed runaway erosion of channel beds which caused very deep main channels and relatively steep channel banks, which likely caused the depth distributions to be unnaturally deep at large δ scales. The braided river model also exhibits depth detected at multiple scales, as in the Waimakariri, because channel depth is not the the only factoring determining δ. Bar height and distance between channels also play a role in determining the δ scale, so differences in these factors lead to channel depths being identified at a range of different scales. Finer resolution modeling with between channel resolution may be required to adequately compare model results to natural systems. Future work should include topographic re-sampling to assess the differences/similarities between numerical models and natural systems at equivalent spatial resolutions.

5.2 Comparison to other methods for channel network extraction

An earlier method based the channel extraction on simplified hydrodynamic modeling and it has been suggested that flow modeling is a better method for quantifying connectivity in channel networks with divergences and convergences than methods utilizing topography [*Limaye*, 2017]. This was largely correct before the present work, when older methods failed in systems with jumps in channel bed elevation (see Introduction). On the other hand, modeling connectivity accounting for the water surface elevation through flow modeling also has some clear advantages over topographic methods. Namely, hydrodynamic schemes can account for the effects of vegetation in determining landscape connectivity. Vegetation plays a major role in controlling water flow especially between channelized and floodplain (over-bank) environments [*Musner et al.*, 2014; *Hiatt and Passalacqua*, 2017; *Wright et al.*, 2018]) which has major effects on channel initiation, erosion, and deposition [*Temmerman et al.*, 2007; *Vandenbruwaene et al.*, 2011; *Nardin and Edmonds*, 2014; *Nardin et al.*, 2016]. Another advantage may be the ability of flow models to capture channel connectivity even when complete bathymetric information is unavailable [e.g., *Limaye*, 2017], which is not possible using topographic methods such as LowPath.

However, there are several distinct advantages of using the topographic method of LowPath versus simplified hydrodynamic models. Most importantly, LowPath relies only on the geomorphic signatures of the system (i.e., the channel network geometry) and is able to identify the channel thalweg in each network link by tracing the lowest elevation paths and is insensitive to local bed jumps. Furthermore, there are neither assumptions required of any hydrodynamic condition nor uncertain parameters such as hydraulic resistance. The recognized thalweg in particular is an important feature of a channelized system. For example, stream-wise flow velocities are often highest above the channel thalweg and lateral flow structure is partly dictated by thalweg position and geometry relative to other channel features [*Valle-Levinson et al.*, 2003; *Blanckaert*, 2011; *Zinger et al.*, 2013; *Konsoer et al.*, 2016], which drives morphodynamic processes such as point bar deposition, channel bend erosion, chute cutoff [e.g., *van Dijk et al.*, 2012]. Thus, proper and objective identification of channel thalwegs from topographic data is an important feature to capture for network extraction that has not been previously available in mutli-threaded systems, because thalweg dynamics are important for multi-thread channel evolution [*Li et al.*, 2017]. Even outside of multi-thread channel applications LowPath represents an advancement in identifying thalweg geometry in single-thread systems, especially in pool-riffle channels that may have local minima in thalweg elevation that are filled via steepest-descent schemes but are captured with LowPath.

Furthermore, the stability and functioning of channel junctions in tidal systems are poorly understood, and the network allows testing of theory developed for rivers independent of flow models. Relative channel depths (i.e., thalweg geometry) are defining characteristics for river bifurcation stability and discharge asymmetry [*Edmonds and Slingerland*, 2008; *Kleinhans et al.*, 2008, 2013; *van Dijk et al.*, 2014; *Bolla Pittaluga et al.*, 2015]. However, estuaries exhibit mutually evasive ebb- and flood-dominated channels connected at bifurcations, and it is unclear why these asymmetrical bifurcations form with a tidal phase dependence and how this affects propagation of changes through the network [*Wang et al.*, 2002; *Kleinhans et al.*, 2015; *Leuven et al.*, 2018; *van Dijk et al.*, 2019].

Another distinct advantage of LowPath over hydrodynamic methods is the capability to automatically and objectively decompose the extracted channel thalwegs into a topologically-coherent network of links and nodes that is represented by an adjacency matrix. While analyses of topological characteristics of estuaries and braided rivers in this paper are limited to relatively simple metrics like node count (Fig. 8), many recent studies have used network analyses of multi-thread channel networks in the geosciences to quantify channel network evolution, vulnerability, and system self-organization [*Marra et al.*, 2014; *Tejedor et al.*, 2015a,b, 2016, 2017, 2018]. Specifically, the pioneering work of *Tejedor et al.* [2015a,b] established a framework for quantifying a suite of metrics that quantify the structural and dynamic connectivities of river delta channel networks using spectral graph theory. The framework relies on the assumption that delta channel networks are purely distributary (i.e., all network links emanate from a single apex node and have seaward transport directions), which cannot be directly applied to systems like estuaries and braided rivers. *Marra et al.* [2014] first attempted to use graph theoretic metrics, specifically the betweenness centrality [*Brandes*, 2001], in a braided river system and identified the importance of channels within three distinct reaches of the Jamuna River. However, there still exists no rigorous framework for addressing topological and dynamic connectivity using graph theory for the non-distributary, chain-like multi-thread channel networks in braided rivers and estuaries. While LowPath represents an advancement in generating the topology of such channel networks, moving the needle forward on understanding dynamics of such channels networks will still require research to establish theoretical tools for network analyses similar to those presented by *Tejedor et al.* [2015a,b] for deltas.

Finally, development of methods that track network development through time would allow tremendous advances in model and data analyses. Though LowPath currently extracts channel networks at sequential timesteps, each extracted network is independent of the previous timestep. This presents a challenge for performing desired morphological analysis such as tracking the nodal point of a bifurcation through time, assessing avulsions, and tracking changes to individual channels. Further development of the network tool requires the possibility to define a single multi-temporal network structure in both space and time and, for application on discrete data, such rigorous measures for similarity that shifting links and nodes are recognized correctly. In turn, the mathematical rules that correctly identify such shifts require phenomenological models of channel behaviour and/or may well capture such natural dynamics.

6 Conclusions

This paper presents a novel method for objectively and automatically extracting topologically-complete networks and geometry from multi-channel environments using only topography and bathymetry data.

The method, called LowPath, relies on extracting the lowest paths traversing a topography across a range of spatial scales, quantified by a new metric for volume-based channel separation in three-dimensional environments called the sand function. The methodology represents a significant advancement over classic steepest-descent-based algorithms for detecting channels from topography, which cannot handle flow divergences and bed steps, which are ubiquitous in multi-channel systems like braided river, deltas, estuaries, and alluvial fans. The method also provides an advantage over inundation-based approaches which cannot capture the full network topology of the extracted channel network. The new channel extraction method represents a unique and important tool for furthering our ability to quantitatively assess channel network structure and geometry in complex environment.

The LowPath method was applied to four case studies: the Western Scheldt estuary, a morphodynamic model of an alluvial estuary, the Waimakariri River, and a morphodynamic model of a braided river. The analyses of the case studies reveal that (1) the number of network links and nodes are inversely related to the sand function scale, (2) the relative lengths of links is positively related to the sand function scale and this relation follows a positive power law with and exponent of $0.23 - 0.35$, and (3) the elevations of links detected at high sand function scales are deeper than those detected at smaller scales. The quantitative and objective comparison of the detailed channel network allows fair comparisons between topological and geometrical characteristics of natural systems and those in numerical morphodynamic models, suggesting that highly braided systems have collectively longer secondary and smaller channel segments than main channel length, as opposed to lower-braided systems where the main channel has a higher length than the collective smaller channels. Furthermore the results suggest that the tendency to incise channels in the models differs from that in nature for braided rivers and estuaries.

Acknowledgments

In theoretical computer science, it is customary to list authors in alphabetical order. Therefore, in reference [*Kleinhans et al.*, 2017], the author order does not necessarily reflect the contributions of the authors. M. Hiatt and M.G. Kleinhans were supported by an ERC Consolidator Grant (agreement 647570) awarded to M.G. Kleinhans. T. Ophelders, W. Sonke, and B. Speckmann were supported by the Netherlands Organisation for Scientific Research (NWO) under project no. 639.023.208 (Vici granted to B. Speckmann), K. Verbeek under project no. 639.021.541 (Veni granted to K. Verbeek) and W.M. van Dijk under project no. 016.140.316 (Vici granted to M.G. Kleinhans). Authors contributed to the following portions of the project: conceptualization (M.H., W.S., E.A.A., M.vK., T.O., K.V., B.S., M.G.K.), formal analysis (M.H., W.S., W.M.vD., T.O., J.V.), funding acquisition (B.S., M.G.K.), methodology (M.H., W.S., W.M.vD.), software (W.S., T.O., K.V.), supervision (B.S., M.G.K.), and manuscript preparation (M.H., W.S., W.M.vD., M.G.K.).

References

Albert, R., and A.-L. Barabási (2002), Statistical mechanics of complex networks, *Rev. Mod. Phys.*, *74*, 47–97, doi:10.1103/RevModPhys.74.47.

Ariza-Villaverde, A., F. Jiménez-Hornero, and E. G. De Ravé (2015), Influence of dem resolution on drainage network extraction: A multifractal analysis, *Geomorphology*, *241*, 243–254.

Ashworth, P., J. Best, and M. Jones (2006), The relationship between channel avulsion, flow occupancy and aggradation in braided rivers: insights from an experimental model, *Sedimentology*, *54*(3), 497–513, doi:10.1111/j.1365-3091.2006.00845.x.

Baar, A. (2019), Impact of small-scale transverse bed slope effects on large-scale morphology : Experimental and modelling studies, Ph.d. dissertation, Utrecht University, Utrecht, Netherlands.

Benda, L., N. L. Poff, D. Miller, T. Dunne, G. Reeves, G. Pess, and M. Pollock (2004), The network dynamics hypothesis: How channel networks structure riverine habitats, *BioScience*, *54*(5), 413–427, doi:10.1641/0006-3568(2004)054[0413:TNDHHC]2.0.CO;2.

Bertoldi, W., L. Zanoni, and M. Tubino (2009), Planform dynamics of braided streams, *Earth Surface Processes and Landforms*, *34*(4), 547–557.

Blanckaert, K. (2011), Hydrodynamic processes in sharp meander bends and their morphological implications, *Journal of Geophysical Research: Earth Surface*, *116*(F1), doi:10.1029/2010JF001806.

Bolla Pittaluga, M., R. Repetto, and M. Tubino (2003), Channel bifurcation in braided rivers: Equilibrium configurations and stability, *Water Resour. Res.*, *39*, 1046, doi:10.1029/2001WR001112.

Bolla Pittaluga, M., G. Coco, and M. G. Kleinhans (2015), A unified framework for stability of channel bifurcations in gravel and sand fluvial systems, *Geophysical Research Letters*, *42*(18), 7521–7536.

Braat, L., T. van Kessel, J. R. F. W. Leuven, and M. G. Kleinhans (2017), Effects of mud supply on large-scale estuary morphology and development over centuries to millennia, *Earth Surface Dynamics*, *5*(4), 617–652, doi:10.5194/esurf-5-617-2017.

Brandes, U. (2001), A faster algorithm for betweenness centrality, *Journal of mathematical sociology*, *25*(2), 163–177.

Church, M. (2006), Bed material transport and the morphology of alluvial river channels, *Annu. Rev. Earth Planet. Sci.*, *34*, 325–354.

Crosato, A., and E. Mosselman (2009), Simple physics-based predictor for the number of river bars and the transition between meandering and braiding, *Water Resources Research*, *45*(3), doi:10.1029/2008WR007242.

Czuba, J. A., and E. Foufoula-Georgiou (2014), A network-based framework for identifying potential synchronizations and amplifications of sediment delivery in river basins, *Water Resources Research*, *50*(5), 3826–3851, doi:10.1002/2013WR014227.

Dai, T., and J. W. Labadie (2001), River basin network model for integrated water quantity/quality management, *Journal of water resources planning and management*, *127*(5), 295–305.

Dillabaugh, C. R., K. O. Niemann, and D. E. Richardson (2002), Semi-automated extraction of rivers from digital imagery, *GeoInformatica*, *6*(3), 263–284, doi:10.1023/A:1019718019825.

Dodds, P. S., and D. H. Rothman (2000), Scaling, universality, and geomorphology, *Annual Review of Earth and Planetary Sciences*, *28*(1), 571–610.

Edelsbrunner, H., J. Harer, and A. Zomorodian (2001), Hierarchical morse complexes for piecewise linear 2-manifolds, in *Proceedings of the Seventeenth Annual Symposium on Computational Geometry*, SCG '01, pp. 70–79, ACM, New York, NY, USA, doi:10.1145/378583.378626.

Edmonds, D., and R. Slingerland (2008), Stability of delta distributary networks and their bifurcations, *Water Resources Research*, *44*(9).

Edmonds, D., C. Paola, D. Hoyal, and B. Sheets (2011), Quantitative metrics that describe river deltas and their channel networks, *J. Geophys. Res.: Earth Surf.*, *116*, F04022, doi:10.1029/2010JF001955.

Egozi, R., and P. Ashmore (2008), Defining and measuring braiding intensity, *Earth Surface Processes and Landforms*, *33*(14), 2121–2138, doi:10.1002/esp.1658.

Fagherazzi, S., A. Bortoluzzi, W. E. Dietrich, A. Adami, S. Lanzoni, M. Marani, and A. Rinaldo (1999), Tidal networks: 1. Automatic network extraction and preliminary scaling features from digital terrain maps, *Water Resources Research*, *35*(12), 3891–3904.

Galloway, W. E. (1975), Process framework for describing the morphologic and stratigraphic evolution of deltaic depositional systems.

Garbrech, J., and L. Mart (1994), Grid size dependency of parameters extracted, *Computers & Geosciences*, *20*(1), 85–87.

Geleynse, N., J. Storms, D. Walstra, R. Jagers, Z. Wang, and M. Stive (2011), Controls on river delta formation; insights from numerical modelling, *Planet. Sci. Lett.*, *302*(1), 217–226, doi:10.1016/j.epsl.2010.12.013.

Germanoski, D., and S. A. Schumm (1993), Changes in braided river morphology resulting from aggradation and degradation, *The Journal of Geology*, *101*(4), 451–466, doi:10.1086/648239.

Hiatt, M., and P. Passalacqua (2017), What controls the transiton from confined to unconfined flow? analysis of hydraulics in a coastal river delta, *J. Hydraul. Engr.*, *143*(6), doi:10.1061/(ASCE)HY.1943-7900.0001309.

Hicks, D. M., M. J. Duncan, S. N. Lane, M. Tal, and R. Westaway (2007), 21 contemporary morphological change in braided gravel-bed rivers: new developments from field and laboratory studies, with particular reference to the influence of riparian vegetation, *Developments in Earth Surface Processes*, *11*, 557–584.

Howard, A. D., M. E. Keetch, and C. L. Vincent (1970), Topological and geometrical properties of braided streams, *Water Resources Research*, *6*(6), 1674–1688, doi:10.1029/WR006i006p01674.

Isikdogan, F., A. Bovik, and P. Passalacqua (2015), Automatic channel network extraction from remotely sensed images by singularity analysis, *IEEE Geoscience and Remote Sensing Letters*, *12*(11), 2218–2221, doi:10.1109/LGRS.2015.2458898.

Isikdogan, F., A. Bovik, and P. Passalacqua (2017), Rivamap: An automated river analysis and mapping engine, *Remote Sensing of Environment*, doi: https://doi.org/10.1016/j.rse.2017.03.044.

Jerolmack, D., and J. Swenson (2007), Scaling relationships and evolution of distributary networks on wave-influenced deltas, *Geophys. Res. Lett.*, *34*, L23402, doi: 10.1029/2007GL031823.

Kleinhans, M., A. Wilburs, and W. ten Brinke (2007), Opposite hysteresis of sand and gravel transport upstream and downstream of a bifurcation during a flood in the River Rhine, the Netherlands, *Neth. J. Geosci.*, *86*, 273–285.

Kleinhans, M., M. van Kreveld, T. Ophelders, W. Sonke, B. Speckmann, and K. Verbeek (2017), Computing representative networks for braided rivers, in *33rd International Symposium on Computational Geometry (SoCG 2017)*, *Leibniz International Proceedings in Informatics (LIPIcs)*, vol. 77, edited by B. Aronov and M. J. Katz, pp. 48:1–48:16, Schloss Dagstuhl–Leibniz-Zentrum fuer Informatik, Dagstuhl, Germany, doi:10.4230/LIPIcs.SoCG.2017.48.

Kleinhans, M. G. (2005), Flow discharge and sediment transport models for estimating a minimum timescale of hydrological activity and channel and delta formation on Mars, *Journal of Geophysical Research: Planets*, *110*(E12), doi: 10.1029/2005JE002521.

Kleinhans, M. G. (2010), Sorting out river channel patterns, *Progress in Physical Geography: Earth and Environment*, *34*(3), 287–326, doi:10.1177/0309133310365300.

Kleinhans, M. G., and J. H. van den Berg (2011), River channel and bar patterns explained and predicted by an empirical and a physicsbased method, *Earth Surface Processes and Landforms*, *36*(6), 721–738, doi:10.1002/esp.2090.

Kleinhans, M. G., C. J. Buskes, and H. W. de Regt (2005), Terra Incognita: explanation and reduction in earth science, *International Studies in the Philosophy of Science*, *19*(3), 289–317.

Kleinhans, M. G., H. R. A. Jagers, E. Mosselman, and C. J. Sloff (2008), Bifurcation dynamics and avulsion duration in meandering rivers by one-dimensional and three-dimensional models, *Water Resources Research*, *44*(8), doi:10.1029/2007WR005912.

Kleinhans, M. G., R. I. Ferguson, S. N. Lane, and R. J. Hardy (2013), Splitting rivers at their seams: bifurcations and avulsion, *Earth Surface Processes and Landforms*, *38*(1), 47–61, doi:10.1002/esp.3268.

Kleinhans, M. G., R. T. van Scheltinga, M. van der Vegt, and H. Markies (2015), Turning the tide: Growth and dynamics of a tidal basin and inlet in experiments, *Journal of Geophysical Research: Earth Surface*, *120*(1), 95–119, doi:10.1002/2014JF003127.

Konsoer, K. M., B. L. Rhoads, J. L. Best, E. J. Langendoen, J. D. Abad, D. R. Parsons, and M. H. Garcia (2016), Three-dimensional flow structure and bed morphology in large elongate meander loops with different outer bank roughness characteristics, *Water Resources Research*, *52*(12), 9621–9641.

Lacroix, M. P., L. W. Martz, G. W. Kite, and J. Garbrecht (2002), Using digital terrain analysis modeling techniques for the parameterization of a hydrologic model, *Environmental Modelling & Software*, *17*(2), 125 – 134, doi:https://doi.org/10.1016/S1364-8152(01)00042-1.

Lashermes, B., E. Foufoula-Georgiou, and W. E. Dietrich (2007), Channel network extraction from high resolution topography using wavelets, *Geophysical Research Letters*, *34*(23).

Leopold, L. B., and M. G. Wolman (1957), *River channel patterns: braided, meandering, and straight*, US Government Printing Office.

Leuven, J., M. Kleinhans, S. Weisscher, and M. van der Vegt (2016), Tidal sand bar dimensions and shapes in estuaries, *Earth-Science Reviews*, *161*, 204–223.

Leuven, J., T. Haas, L. Braat, and M. Kleinhans (2017), Topographic forcing of tidal sand bar patterns for irregular estuary planforms, *Earth Surface Processes and Landforms*.

Leuven, J. R. F. W., L. Braat, W. M. van Dijk, T. de Haas, E. P. van Onselen, B. G. Ruessink, and M. G. Kleinhans (2018), Growing forced bars determine nonideal estuary planform, *Journal of Geophysical Research: Earth Surface*, *123*(11), 2971–2992, doi:10.1029/2018JF004718.

Li, J., J. Xia, M. Zhou, S. Deng, and X. Zhang (2017), Variation in reach-scale thalweg-migration intensity in a braided reach of the lower Yellow River in 19862015, *Earth Surface Processes and Landforms*, *42*(13), 1952–1962, doi:10.1002/esp.4154.

Liang, M., C. Van Dyk, and P. Passalacqua (2016), Quantifying the patterns and dynamics of river deltas under conditions of steady forcing and relative sea level rise, *Journal of Geophysical Research: Earth Surface*, *121*(2), 465–496, doi:10.1002/2015JF003653, 2015JF003653.

Limaye, A. B. (2017), Extraction of multithread channel networks with a reduced-complexity flow model, *Journal of Geophysical Research: Earth Surface*, doi:10.1002/2016JF004175, 2016JF004175.

Maidment, D. R. (2016), Conceptual framework for the National Flood Interoperability Experiment, *JAWRA Journal of the American Water Resources Association*, *53*(2), 245–257, doi:10.1111/1752-1688.12474.

Marra, W. A., M. G. Kleinhans, and E. A. Addink (2014), Network concepts to describe channel importance and change in multichannel systems: test results for the jamuna river, bangladesh, *Earth Surface Processes and Landforms*, *39*(6), 766–778, doi:10.1002/esp.3482, eSP-12-0168.R2.

Millar, R. G. (2000), Influence of bank vegetation on alluvial channel patterns, *Water Resources Research*, *36*(4), 1109–1118.

Molnar, D., and P. Julien (2000), Grid-size effects on surface runoff modeling, *Journal of Hydrologic Engineering*, *5*(1), 8–16.

Montgomery, D. R., and W. E. Dietrich (1989), Source areas, drainage density, and channel initiation, *Water Resources Research*, *25*(8), 1907–1918, doi:10.1029/WR025i008p01907.

Musner, T., A. Bottacin-Busolin, M. Zaramella, and A. Marion (2014), A contaminant transport model for wetlands accounting for distinct residence time bimodality, *Journal of Hydrology*, *515*, 237 – 246, doi:http://dx.doi.org/10.1016/j.jhydrol.2014.04.043.

Nardin, W., and D. Edmonds (2014), Optimum vegetation height and density for inorganic sedimentation in deltaic marshes, *Nature Geoscience*, *7*, 722–726, doi:10.1038/ngeo2233.

Nardin, W., D. Edmonds, and S. Fagherazzi (2016), Influence of vegetation on spatial patterns of sediment deposition in deltaic islands during flood, *Advances in Water Resources*, *93, Part B*, 236 – 248, doi:http://dx.doi.org/10.1016/j.advwatres.2016.01.001.

Newman, M. (2010), *Networks: an introduction*, Oxford university press.

Newman, M. E. J. (2003), The structure and function of complex networks, *SIAM Review*, *45*(2), 167–256, doi:10.1137/S003614450342480.

Nienhuis, J. H., A. Ton Hoitink, and T. E. Törnqvist (2018), Future change to tide-influenced deltas, *Geophysical Research Letters*.

Nittrouer, J. A., J. Shaw, M. P. Lamb, and D. Mohrig (2011), Spatial and temporal trends for water-flow velocity and bed-material sediment transport in the lower Mississippi River, *Geological Society of America Bulletin*, doi:10.1130/B30497.1.

Orton, G., and H. Reading (1993), Variability of deltaic processes in terms of sediment supply, with particular emphasis on grain size, *Sedimentology*, *40*(3), 475–512.

Passalacqua, P., T. Do Trung, E. Foufoula-Georgiou, G. Sapiro, and W. E. Dietrich (2010), A geometric framework for channel network extraction from lidar: Nonlinear diffusion and geodesic paths, *Journal of Geophysical Research: Earth Surface*, *115*(F1).

Passalacqua, P., S. Lanzoni, C. Paola, and A. Rinaldo (2013), Geomorphic signatures of deltaic processes and vegetation: The Ganges-Brahmaputra-Jamuna case study, *J. Geophys. Res. Earth Surf.*, *118*, 1838 – 1849, doi:10.1002/jgrf.20128.

Passalacqua, P., P. Belmont, D. M. Staley, J. D. Simley, J. R. Arrowsmith, C. A. Bode, C. Crosby, S. B. DeLong, N. F. Glenn, S. A. Kelly, et al. (2015), Analyzing high resolution topography for advancing the understanding of mass and energy transfer through landscapes: A review, *Earth-Science Reviews*, *148*, 174–193.

Pavelsky, T. M., and L. C. Smith (2008), RivWidth: A software tool for the calculation of river widths from remotely sensed imagery, *IEEE Geoscience and Remote Sensing Letters*, *5*(1), 70–73, doi:10.1109/LGRS.2007.908305.

Pelletier, J. D. (2013), A robust, twoparameter method for the extraction of drainage networks from highresolution digital elevation models (dems): Evaluation using synthetic and realworld dems, *Water Resources Research*, *49*(1), 75–89, doi:10.1029/2012WR012452.

Pelletier, J. D. (204), Persistent drainage migration in a numerical landscape evolution model, *Geophysical Research Letters*, *31*(20), doi:10.1029/2004GL020802.

Phillips, C. B., and D. J. Jerolmack (2016), Self-organization of river channels as a critical filter on climate signals, *Science*, *352*(6286), 694–697, doi:

10.1126/science.aad3348.

Redolfi, M., M. Tubino, W. Bertoldi, and J. Brasington (2016), Analysis of reach-scale elevation distribution in braided rivers: Definition of a new morphologic indicator and estimation of mean quantities, *Water Resources Research*, *52*(8), 5951–5970, doi:10.1002/2015WR017918.

Robinson, A. H. W. (1960), Ebb-flood channel systems in sandy bays and estuaries, *Geography*, *45*(3), 183–199.

Rodriguez-Iturbe, I., and A. Rinaldo (Eds.) (1997), *Fractal River Basins: Chance and Self-Organization*, 1st ed., 547 pp., Cambridge University Press, New York, NY.

Rossi, V., W. Kim, J. Leva-Lopez, D. Edmonds, N. Geleynse, C. Olariu, R. Steel, M. Hiatt, and P. Passalacqua (2016), Impact of tidal currents on delta-channel deepening, stratigraphic architecture and sediment bypass beyond the shoreline, *Geology*, doi:doi:10.1130/G38334.1, accepted.

Sangireddy, H., C. P. Stark, A. Kladzyk, and P. Passalacqua (2016a), Geonet: An open source software for the automatic and objective extraction of channel heads, channel network, and channel morphology from high resolution topography data, *Environmental Modelling & Software*, *83*, 58 – 73, doi: https://doi.org/10.1016/j.envsoft.2016.04.026.

Sangireddy, H., R. A. Carothers, C. P. Stark, and P. Passalacqua (2016b), Controls of climate, topography, vegetation, and lithology on drainage density extracted from high resolution topography data, *Journal of Hydrology*, *537*, 271–282.

Schuurman, F., and M. G. Kleinhans (2015), Bar dynamics and bifurcation evolution in a modelled braided sand-bed river, *Earth Surface Processes and Landforms*, *40*(10), 1318–1333, doi:10.1002/esp.3722, esp.3722.

Schuurman, F., W. A. Marra, and M. G. Kleinhans (2013), Physics-based modeling of large braided sand-bed rivers: Bar pattern formation, dynamics, and sensitivity, *Journal of Geophysical Research: Earth Surface*, *118*(4), 2509–2527, doi: 10.1002/2013JF002896.

Shelef, E., and G. E. Hilley (2013), Impact of flow routing on catchment area calculations, slope estimates, and numerical simulations of landscape development, *Journal of Geophysical Research: Earth Surface*, *118*(4), 2105–2123, doi:10.1002/jgrf.20127.

Shivashankar, N., S. M, and V. Natarajan (2012), Parallel computation of 2d morse-smale complexes, *IEEE Transactions on Visualization and Computer Graphics*, *18*(10), 1757–1770, doi:10.1109/TVCG.2011.284.

Smart, J., and V. Moruzzi (1972), Quantitative properties of delta channel networks, *Z. Geomorph.*, *16*(3), 283–300.

Tal, M., and C. Paola (2010), Effects of vegetation on channel morphodynamics: results and insights from laboratory experiments, *Earth Surface Processes and Landforms*, *35*(9), 1014–1028.

Tal, M., K. Gran, A. B. Murray, C. Paola, and D. M. Hicks (2004), Riparian vegetation as a primary control on channel characteristics in multi-thread rivers, *Riparian vegetation and fluvial geomorphology*, pp. 43–58.

Tarboton, D. G. (1997), A new method for the determination of flow directions and upslope areas in grid digital elevation models, *Water Resources Research*, *33*(2), 309–319, doi:10.1029/96WR03137.

Tarboton, D. G., and D. P. Ames (2001), *Advances in the Mapping of Flow Networks from Digital Elevation Data*, ASCE, doi:10.1061/40569(2001)166.

Tarboton, D. G., R. L. Bras, and I. RodriguezIturbe (1991), On the extraction of channel networks from digital elevation data, *Hydrological Processes*, *5*(1), 81–100, doi:10.1002/hyp.3360050107.

Tarolli, P. (2014), High-resolution topography for understanding earth surface processes: Opportunities and challenges, *Geomorphology*, *216*, 295 – 312, doi: https://doi.org/10.1016/j.geomorph.2014.03.008.

Tejedor, A., A. Longjas, I. Zaliapin, and E. Foufoula-Georgiou (2015a), Delta channel networks: 1. a graph-theoretic approach for studying connectivity and steady state transport on deltaic surfaces, *Water Resources Research*, *51*(6), 3998–4018, doi:10.1002/2014WR016577.

Tejedor, A., A. Longjas, I. Zaliapin, and E. Foufoula-Georgiou (2015b), Delta channel networks: 2. metrics of topologic and dynamic complexity for delta comparison, physical inference, and vulnerability assessment, *Water Resources Research*, *51*(6), 4019–4045, doi:10.1002/2014WR016604.

Tejedor, A., A. Longjas, R. Caldwell, D. A. Edmonds, I. Zaliapin, and E. Foufoula-Georgiou (2016), Quantifying the signature of sediment composition on the topologic and dynamic complexity of river delta channel networks and inferences toward delta classification, *Geophysical Research Letters*, *43*(7), 3280–3287, doi:10.1002/2016GL068210, 2016GL068210.

Tejedor, A., A. Longjas, D. A. Edmonds, I. Zaliapin, T. T. Georgiou, A. Rinaldo, and E. Foufoula-Georgiou (2017), Entropy and optimality in river deltas, *Proceedings of the National Academy of Sciences*, *114*(44), 11,651–11,656.

Tejedor, A., A. Longjas, P. Passalacqua, Y. Moreno, and E. Foufoula-Georgiou (2018), Multiplex networks: A framework for studying multiprocess multiscale connectivity via coupled-network theory with an application to river deltas, *Geophysical Research Letters*, *45*(18), 9681–9689.

Temmerman, S., T. Bouma, J. Van de Koppel, D. Van der Wal, M. De Vries, and P. Herman (2007), Vegetation causes channel erosion in a tidal landscape, *Geology*, *35*(7), 631–634, doi:10.1130/G23502A.1.

Townend, I. (2012), The estimation of estuary dimensions using a simplified form model and the exogenous controls, *Earth Surface Processes and Landforms*, *37*(15), 1573–1583, doi:https://doi.org/10.1002/esp.3256.

Valle-Levinson, A., C. Reyes, and R. Sanay (2003), Effects of bathymetry, friction, and rotation on estuaryocean exchange, *Journal of Physical Oceanography*, *33*(11), 2375–2393, doi:10.1175/1520-0485(2003)033¡2375:EOBFAR¿2.0.CO;2.

Van den Berg, J. H. (1995), Prediction of alluvial channel pattern of perennial rivers, *Geomorphology*, *12*(4), 259–279.

Van der Wegen, M., and J. Roelvink (2012), Reproduction of estuarine bathymetry by means of a process-based model: Western Scheldt case study, the Netherlands, *Geomorphology*, *179*, 152–167.

van Dijk, W. M., W. I. van de Lageweg, and M. G. Kleinhans (2012), Experimental meandering river with chute cutoffs, *Journal of Geophysical Research: Earth Surface*, *117*(F3), doi:10.1029/2011JF002314.

van Dijk, W. M., F. Schuurman, W. I. van de Lageweg, and M. G. Kleinhans (2014), Bifurcation instability and chute cutoff development in meandering gravel-bed rivers, *Geomorphology*, *213*, 277 – 291, doi:https://doi.org/10.1016/j.geomorph.2014.01.018.

van Dijk, W. M., D. R. Mastbergen, G. A. van den Ham, J. R. F. W. Leuven, and M. G. Kleinhans (2018), Location and probability of shoal margin collapses in a sandy estuary, *Earth Surface Processes and Landforms*, *43*(11), 2342–2357, doi:10.1002/esp.4395.

van Dijk, W. M., M. R. Hiatt, J. J. van der Werf, and M. G. Kleinhans (2019), Effects of shoal margin collapses on the morphodynamics of a sandy estuary, *Journal of Geophysical Research: Earth Surface*, *0*(0), doi:10.1029/2018JF004763.

van Veen, J. (1950), Eb- en vloedschaar systemen in de Nederlandse getijwateren, *Journal of the Royal Dutch Geographical Society*, *67*, 303–325, in Dutch.

Vandenbruwaene, W., S. Temmerman, T. J. Bouma, P. C. Klaassen, M. B. de Vries, D. P. Callaghan, P. van Steeg, F. Dekker, L. A. van Duren, E. Martini, T. Balke, G. Biermans, J. Schoelynck, and P. Meire (2011), Flow interaction with dynamic vegetation patches: Implications for biogeomorphic evolution of a tidal landscape, *Jour-*

nal of Geophysical Research: Earth Surface, *116*(F1), doi:10.1029/2010JF001788.

Verbeek, H., F. Tank, and M. Groenewoud (1998), Drempels in de westerschelde (in Dutch), *Technical report*, Rijksinstituut voor kust en zee (RIKZ).

Wang, Z., M. Jeuken, H. Gerritsen, H. de Vriend, and B. Kornman (2002), Morphology and asymmetry of the vertical tide in the Westerschelde estuary, *Continental Shelf Research*, *22*(17), 2599 – 2609, doi:https://doi.org/10.1016/S0278-4343(02)00134-6.

Welber, M., W. Bertoldi, and M. Tubino (2012), The response of braided planform configuration to flow variations, bed reworking and vegetation: the case of the Tagliamento River, Italy, *Earth Surface Processes and Landforms*, *37*(5), 572–582, doi:10.1002/esp.3196.

Wickert, A. D., J. M. Martin, M. Tal, W. Kim, B. Sheets, and C. Paola (2013), River channel lateral mobility: metrics, time scales, and controls, *Journal of Geophysical Research: Earth Surface*, *118*(2), 396–412, doi:10.1029/2012JF002386.

Wright, K., M. Hiatt, and P. Passalacqua (2018), Hydrological connectivity in vegetated river deltas: The importance of patchiness below a threshold, *Geophysical Research Letters*, *45*(19), 10,416–10,427, doi:10.1029/2018GL079183.

Zinger, J. A., B. L. Rhoads, J. L. Best, and K. K. Johnson (2013), Flow structure and channel morphodynamics of meander bend chute cutoffs: A case study of the Wabash River, USA, *Journal of Geophysical Research: Earth Surface*, *118*(4), 2468–2487.

Zolezzi, G., W. Bertoldi, and M. Tubino (2006), Morphological analysis and prediction of river bifurcations, in *Braided Rivers: Process, Deposits, Ecology and Management*, *Special Publication Number 36 of the International Association of Sedimentologists*, vol. 36, edited by G. Sambrock Smith, J. Best, C. Bristow, and G. Petts, pp. 233–256, Blackwell Publishing Ltd., Oxford, UK, doi:10.1002/9781444304374.ch11.